

Chapter 5

Parsec-Scale Jets in Active Galactic Nuclei

Denise C. Gabuzda

Abstract Considerable progress has been made over the past decade or so in understanding the jets of Active Galactic Nuclei on the parsec scales probed by Very Long Baseline Interferometry. The availability of multi-wavelength polarization VLBI observations for relatively large samples of objects for the first time has provided fundamental new information about the spectral indices and Faraday rotation measures in the core and jet components. Reliable estimates of the core magnetic fields and degrees of circular polarization have also become available for the first time. The jets exhibit complex behaviour, such as accelerations and non-radial motions of individual moving features, and even swings of the jet as a whole. New approaches have been developed to estimate the intrinsic speeds and viewing angles of the jets. A variety of new evidence seems to be suggesting that many of the properties we are observing are a consequence of helical magnetic fields carried outward by the jets, which should come about naturally due to the rotation of the central black hole and its accretion disk together with the jet outflow.

5.1 Introduction

The central regions of powerful Active Galactic Nuclei (AGN) radiate huge amounts of energy; the strongest AGN are about 10^5 times more luminous than an entire normal galaxy such as the Milky Way. The source of this phenomenal energy is believed to be the gravitational energy released by matter accreting onto a supermassive ($\sim 10^9$ times the mass of the Sun) black hole at the galactic centre.

About 10–15 % or so of all AGN are “radio-loud,” while the remaining are “radio-quiet.” The generally accepted definition of a radio-loud AGN is that the ratio of its radio (5 GHz) to its optical (B-band) flux be ≥ 10 (Kellermann et al. 1989a). The radio emission is predominantly associated with jets ejected from the central region of the AGN and the lobes that they inflate, suggesting that jets are either

D.C. Gabuzda (✉)
Department of Physics, University College Cork, Cork, Ireland
e-mail: d.gabuzda@ucc.ie

absent or much weaker in the radio-quiet AGN. This radio emission is synchrotron radiation emitted by relativistic electrons moving through regions with magnetic (\mathbf{B}) field; the jets presumably create conditions where both electrons can be accelerated to high energies and magnetic fields can be generated and amplified.

It is natural to strive to image AGN with high resolution, to obtain information about regions close to the central energy source. An extremely powerful tool for studies of radio-loud AGN is Very Long Baseline Interferometry (VLBI), in which radio telescopes around the world are used in synchrony to obtain images with angular resolutions of the order of a milliarcsecond on the sky, or of order a parsec at the cosmological distances characteristic of AGN. Various arrays of radio telescopes around the world are outfitted to carry out VLBI observations, such as the American Very Long Baseline Array (VLBA) and the European VLBI Network (EVN).

Most or all of the radio emission of AGN is associated with jets of plasma that emerge from their central regions, presumably along the rotational axis of the central supermassive black hole. These jets are present on the smallest scales that can be probed with VLBI, and sometimes extend out to scales of many kiloparsecs (see Chap. 3). The synchrotron radiation given off by each individual electron is highly concentrated in the direction of motion of the electron, and the radiation observed for an ensemble of relativistic electrons will, in general, be linear polarized if the synchrotron \mathbf{B} field is at least partially ordered. Linear-polarization observations can thus provide direct information about the degree of order and orientation of the \mathbf{B} field giving rise to the observed synchrotron radiation, and thus play a key role in studies of the conditions in and around AGN jets.

Section 5.2 summarizes the main relativistic effects that directly affect VLBI observations of AGN jets. Section 5.3 provides a brief overview of some basic properties of incoherent synchrotron radiation, and Sect. 5.4 a basic overview of various theoretical models and processes, that feed into interpretations of VLBI observations of AGN jets. Finally, Sect. 5.5 provides a review of the current observations of AGN jets, focusing on recent results and progress.

5.2 Relativistic Effects Influencing the Observations

5.2.1 Aberration and Relativistic Beaming

The Lorentz transformations relating the coordinates of an object in one frame (unprimed) and in another frame (primed) moving relative to the first frame with a relative velocity \mathbf{v} can be used to find the corresponding transformations between the components of the object's velocity parallel and perpendicular to the direction of the relative motion of the two frames.

For light (a photon), the angles θ and θ' along which the light is observed to propagate in the two frames are related by the equations

$$\tan \theta = \frac{\sin \theta'}{\Gamma(\cos \theta' + \beta)} \quad \cos \theta = \frac{\cos \theta' + \beta}{1 + \beta \cos \theta'} \quad (5.1)$$

where β is the jet velocity divided by the speed of light and Γ is the corresponding bulk Lorentz factor. Thus, a photon emitted at right angles to \mathbf{v} in its rest frame ($\theta' = \pi/2$) is observed at the angle

$$\tan \theta = \frac{1}{\Gamma\beta} \quad \cos \theta = \beta \quad \sin \theta = \frac{1}{\Gamma} \quad (5.2)$$

This is the well-known *beaming* of the source radiation in the forward direction of its motion. When Γ is large, $\sin \theta$ will be small, and $\theta \simeq \frac{1}{\Gamma}$. Thus, half the radiation emitted by an isotropically radiating, relativistically moving source is observed within a narrow cone of half-angle $1/\Gamma$.

This *Doppler beaming* or *Doppler boosting* is believed to explain the one-sided appearance of the relativistic jets of AGN on VLBI scales (Sect. 5.5.1). It is believed that, in reality, there are two jets – one approaching (Doppler boosted) and one receding (Doppler dimmed) – if the boosting factor is high enough, the receding jet (whose radiation is beamed in the direction away from the Earth) becomes undetectable.

The difference in the observed direction of propagation of a photon in two frames moving relative to one another is referred to as aberration. Due to aberration, photons we detect arriving from a jet viewed at a small angle to our line of sight were actually emitted by the jet roughly perpendicular to the direction of its motion; thus, we may receive an approximately “side-on” view of the jet, even though we are viewing the jet at a small angle to its axis. This important effect is often neglected when interpreting images of VLBI jets, as will be discussed further below. In addition, when the viewing angle $\theta < 1/\Gamma$, then $\theta' < 90^\circ$, and we have a “head-on” view of the object; whereas $\theta' > 90^\circ$ when $\theta > 1/\Gamma$, and we have a “tail-on” view of the object. In other words, in the latter case, we are actually detecting photons emitted by the source roughly away from the direction toward the Earth. Taking into account the fact that jets viewed at smaller angles will appear brighter, and therefore be more prominently represented in observational samples, the most probable viewing angle for an AGN jet is about $0.6/\Gamma$ (Cohen et al. 2007), but some of the relativistic jets observed in AGN will also be viewed at angles $\theta > 1/\Gamma$, so that we are receiving a “tail-on” view; this will certainly affect observations of these objects – although unfortunately, we cannot be sure which ones they are.

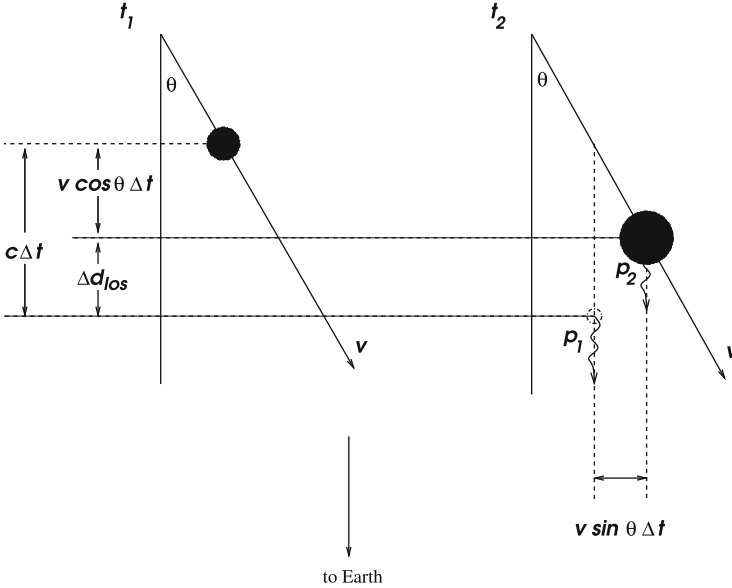


Fig. 5.1 Geometry for superluminal motion

5.2.2 Superluminal Motions

Consider the motion of a clump of plasma in a jet roughly toward the Earth at two times t_1 and t_2 . The angle of the clump's motion relative to the direction toward the Earth is θ , and the clump's velocity is v (Fig. 5.1).

The distance travelled by the clump toward the Earth between the two times is $v \cos \theta \Delta t$, where $\Delta t = t_2 - t_1$. The distance travelled by a photon emitted at t_1 in the time Δt is just $c \Delta t$. The distance between the photons p_1 and p_2 will be $c \Delta t - v \cos \theta \Delta t$, and so the measured time between the arrival of photons p_1 and p_2 emitted at time t_1 and t_2 will be $\Delta t_{meas} = (1 - \beta \cos \theta) \Delta t$, where $\beta = v/c$. The observed distance travelled by the clump in the plane of the sky will be $d_{sky} = v \sin \theta \Delta t$. Thus, the apparent speed of the clump in the plane of the sky will be

$$\beta_{app} = \frac{\Delta d_{sky}}{c \Delta t_{meas}} = \frac{\beta \sin \theta}{1 - \beta \cos \theta} \quad (5.3)$$

The maximum of this function can be found by taking its derivative and setting it equal to zero. This yields a maximum when

$$\cos \theta_{max} = \beta \quad \sin \theta_{max} = \frac{1}{\Gamma} \quad (5.4)$$

or $\theta_{max} = 1/\Gamma$ when Γ is large and θ_{max} is therefore small. The corresponding maximum apparent speed in the plane of the sky is $\beta_{max} = \beta\Gamma$.

Clearly, the observed motion will be superluminal, or apparently faster than light, for sufficiently high intrinsic speeds β and sufficiently small viewing angles $\theta \sim 1/\Gamma$. This provides a simple explanation of superluminal motions in AGN jets, which are very common; unfortunately, it is not possible to unambiguously disentangle the contributions of β and θ to the observed speeds. Nevertheless, studies of superluminal jet component speeds for samples of AGN are extremely useful in determining the nature of differences between different types of AGN, for example.

5.2.3 Measured Variation Timescales and the Doppler Factor

As was noted above, the measured time between the arrival of two photons emitted by a source moving toward the observer at two times separated by Δt is $\Delta t_{meas} = (1 - \beta \cos \theta)\Delta t$. Here, Δt is the time interval in the frame of the observer, and will differ from the time interval between the emission of the two photons in the rest frame of the source (which we denote with a prime) due to relativistic time dilation: $\Delta t = \Gamma\Delta t'$. Therefore,

$$\Delta t_{meas} = (1 - \beta \cos \theta)\Gamma\Delta t \equiv \frac{1}{D}t' \quad (5.5)$$

The inferred time interval between the arrival of the two photons will be too small by a factor

$$D = \frac{1}{\Gamma(1 - \beta \cos \theta)} \quad (5.6)$$

The *Doppler factor* D relates quantities in the rest frame of the source and the observer's frame, taking into account both special relativistic effects and the direction of the source's motion relative to the observer. For example, if θ is small enough that $\cos \theta \simeq 1$ and in addition $\beta \simeq 1$ (highly relativistic motion nearly directly toward the Earth), $\Delta t_{meas} \simeq \frac{1}{2\Gamma}\Delta t'$; i.e., the observer would infer a time between the emission of the two photons that is much too short, by a factor of $1/2\Gamma$.

5.3 Theory of Radio Synchrotron Emission: Potential Observational Manifestations

A review of some basic properties of synchrotron radiation is given in Sect. 4.2.1. The following sections consider some other properties of synchrotron radiation that are particularly relevant for VLBI polarization observations. More detailed

information about synchrotron radiation can be found, for example, in the textbooks by Longair (2010) and Rybicki and Lightman (1979).

5.3.1 Optical Depth

Roughly speaking, if the mean-free-path of a photon in the radiating region is larger than the size of the region, the photon is likely to be able to pass through the region without being absorbed, and we say the region is *optically thin*. If the mean-free-path of a photon is appreciably less than the size of the region, the photon is likely to be absorbed before it leaves the source region, and we say the region is *optically thick*. It turns out that, after integrating over an ensemble of electrons with a power-law electron energy distribution, $N(E)dE \sim E^{-p}dE$, the power radiated at frequency ν in the optically thin part of the spectrum is also a power law proportional to ν^α , where $\alpha = -(p - 1)/2$ is called the *spectral index*.

At low frequencies, there can be appreciable absorption of the synchrotron radiation by the radiating electrons themselves, referred to as *synchrotron self absorption*. This makes the radiating region optically thick at these frequencies; it turns out that this gives rise to a slope of $+5/2$ in this part of the spectrum. A sketch of the total spectrum for a single homogeneous synchrotron-radiating region is shown in Fig. 5.2. The theoretical optically thick spectral index is $+5/2$; the optically thin spectral index is $\alpha = -(p - 1)/2$. The theoretical optically thick spectral index of $+5/2$ is observed very rarely; observed regions are probably usually only partially optically thick (opaque).

Generally speaking, we expect the emission in the core region to be at least partially optically thick, and the emission in the jet to be optically thin.

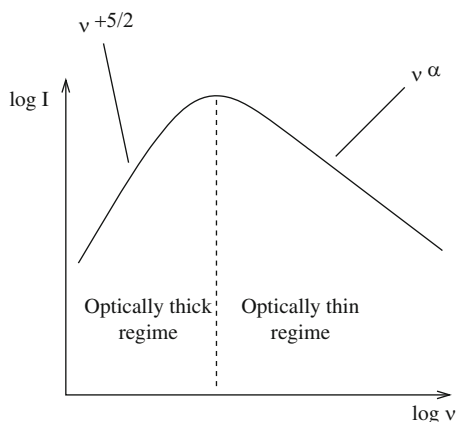


Fig. 5.2 Schematic of the spectrum of a homogeneous source of synchrotron radiation

5.3.2 Linear Polarization

Synchrotron radiation is intrinsically linearly polarized; to obtain 100% polarization, one would have to have a perfectly ordered \mathbf{B} field and an ensemble of electrons which all have the same pitch angle relative to this \mathbf{B} field, corresponding to motion purely in a plane perpendicular to the field, in a region that was optically thin. Although various physical processes can give rise to highly ordered \mathbf{B} fields, it is generally believed that the distribution of pitch angles for the ensemble of radiating electrons is most likely to be uniform and random, i.e. that we are dealing with “incoherent” synchrotron radiation. The degree of polarization m_{thin} expected for such an ensemble of electrons moving in a completely uniform \mathbf{B} field in an optically thin region is given by

$$m_{thin} = \frac{p + 1}{p + 7/3} \quad (5.7)$$

where p is the index of the power law distribution of the electron energies (Pacholczyk 1970). This yields $m_{thin} \simeq 70 - 75\%$ for p values of 2 – 3, which correspond to optically thin spectral indices $\alpha = -0.5$ to -1 , which are fairly typical of the observed spectral indices in the VLBI jets of AGN. The maximum theoretical degree of polarization for the synchrotron radiation associated with AGN jets is usually taken to be about 75%.

The corresponding maximum degree of polarization m_{thick} expected for an optically thin region is given by

$$m_{thick} = \frac{3}{6p + 13}, \quad (5.8)$$

yielding values $m_{thick} \simeq 10 - 12\%$ for p values of 2 – 3 (Pacholczyk 1970).

We can think of the radiation as having two components to its linear polarization: one with its polarization \mathbf{E} vector orthogonal to the magnetic field, and the other with its polarization \mathbf{E} vector aligned with the magnetic field. The former of these two dominates when the radiation is optically thin – qualitatively, this corresponds to \mathbf{E} being in the plane of gyration of the electrons. Recall that the radiation will be optically thick when there is a high probability of a synchrotron photon being absorbed before it can leave the region in which it was radiated. In this regime, the component of the linear polarization that has the higher probability of being absorbed is precisely the one that had the higher probability of being emitted in the optically thin regime – the one with \mathbf{E} perpendicular to the synchrotron \mathbf{B} field. The other component of the polarization – with \mathbf{E} parallel to the \mathbf{B} field – is less likely to be absorbed, and so more likely to be able to leave the emission region.

Thus, in the optically thin regime, the observed plane of polarization is *perpendicular* to the \mathbf{B} field and the degree of linear polarization can reach $\simeq 75\%$, while, in the optically thick regime, the observed plane of polarization is *parallel* to the \mathbf{B} field and the degree of linear polarization is of order 10–12%. In both cases, the degree of polarization will decrease if the local \mathbf{B} field is not completely ordered. The reason for the lower degree of polarization for the optically thick regime is that the component of the polarization with \mathbf{E} parallel to \mathbf{B} is less likely to be emitted, so the total fraction of synchrotron photons emitting this component is modest. Cawthorne and Hughes (2013) have recently pointed out that the optical depth τ at which the 90° rotation in polarization angle in the transition from optically thick to optically thin occurs is actually appreciably greater than $\tau \approx 1$.

5.3.3 Circular Polarization

The degree of circular polarization of incoherent synchrotron radiation is given by

$$m_c = \epsilon_\alpha^v \left(\frac{\nu_{B\perp}}{\nu} \right)^{0.5} \frac{B_{u,los}}{B_\perp^{rms}} \propto \nu^{-0.5} \quad (5.9)$$

where ϵ_α^v is a constant that has values near unity for spectral indices near 0 (as is the case, for example, for most observed VLBI cores at centimeter wavelengths); $B_{u,los}$ is the component of the uniform magnetic field that is responsible for generating the circular polarization; B_\perp^{rms} is the mean field component in the plane of the sky, which includes both the transverse part of the total uniform magnetic field B_u and any disordered field (which contributes to total intensity but not circular polarization); and $\nu_{B\perp} = 2.8 B_\perp^{rms}$ is the gyrofrequency for B_\perp^{rms} in MHz (Legg and Westfold 1968). Thus, the degree of circular polarization associated with the synchrotron mechanism is expected to grow with decreasing frequency. Since the jets of AGN are typically linearly polarized about 10% on parsec scales, a reasonable estimate is $B_{u,los}/B_\perp^{rms} \approx 0.10$; estimating as well $B_\perp^{rms} \approx 0.10$ G, consistent with estimates of the VLBI core magnetic fields (e.g. O’Sullivan and Gabuzda 2009; Pushkarev et al. 2012) suggests that one might obtain m_c values up to about 0.10–0.20% at 5–15 GHz.

5.4 Standard Jet Theory: An Observer’s View

5.4.1 Blandford–Königl Jets: The Nature of the VLBI Core

The generally accepted overall framework for the interpretation of observations of the VLBI jets of AGN is provided by the model proposed by Blandford and Königl (1979). In this model, the jets are taken to be conical, and the feature observed as

the VLBI “core” is interpreted as the “photosphere” of the jet, within which the emission regions are optically thick and outside which they are optically thin. This is usually referred to as the $\tau = 1$ surface, although there is no strict reason that the optical depth at this location must be precisely equal to unity, and this term is essentially conveying the idea that the probability of an emitted photon escaping the emission region is beginning to deviate appreciably from the optically thin probability near zero in this region.

The location of this surface, i.e., the observed location of the VLBI core, depends on the observing frequency, and moves further down the jet at increasingly lower frequencies, as is shown in the schematic in Fig. 5.3. In contrast, the positions of optically thin features in the jet should coincide at different frequencies.

However, absolute position information is lost during the mapping process, and the phase center (coordinate origin) of a VLBI image will tend to coincide with the dominant partially optically thick VLBI core. Therefore, VLBI images obtained at different frequencies will, in general, not be correctly aligned in a physical sense, and cannot be directly superposed, for example, to derive spectral-index maps. To correctly align images obtained at different frequencies, it is necessary to shift them so that the positions of optically thin features coincide at the different frequencies. A variety of techniques for achieving this alignment have been exploited, most importantly model-fitting in the visibility domain to determine the positions of optically thin jet features, which are then made to coincide at different frequencies, and cross-correlation of the optically thin parts of total intensity images (e.g. Walker et al. 2000; Croke and Gabuzda 2008). In practice, different approaches may work best for different types of source structures, and both of these general approaches can yield reliable alignments in particular cases.

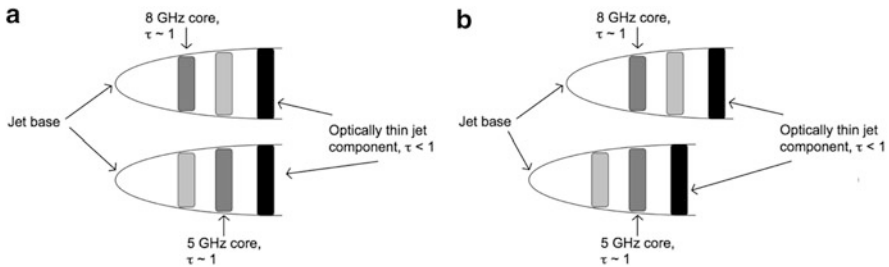


Fig. 5.3 Schematic of a Blandford-Königl jet, where the observed VLBI core corresponds approximately to the $\tau = 1$ surface in the jet at a given frequency. The same jet as observed at 8 GHz (upper jet in each panel) and 5 GHz (lower jet in each panel) is shown; in each graphic, the *black feature* represents an optically thin jet component, the *dark gray feature* the core position at the given frequency, and the *light gray feature* the core position at the other frequency. In panel (a), the jets observed at the two frequencies are correctly aligned, with the optically thin jet component coincident; in panel (b), the jets observed at the two frequencies are incorrectly aligned due to the mapping processes, which tends to place the observed core very close to the map phase center

5.4.2 Shocks

The presence of shocks in VLBI jets has often been invoked as an explanation for the sometimes rapid variability exhibited by AGN. The formation of both forward and reverse shocks has also been demonstrated in numerical simulations of the propagation of a perturbation down a relativistic jet (e.g. Aloy et al. 1999, 2000, 2003; Mimica and Aloy 2010, 2012).

In a region subject to shock compression, the \mathbf{B} field is amplified in the plane of compression, giving rise to appreciable degrees of polarization and a net magnetic field lying in the plane of compression, even in the case of an initially completely tangled magnetic field (Laing 1980; Hughes et al. 1985). In a transverse shock, the plane of compression is perpendicular to the jet direction, the net magnetic field in the shocked region is also perpendicular to the jet direction, and the observed polarization is aligned with the jet direction, assuming the shock region is optically thin.

The polarization expected from oblique and conical shocks has been investigated by Cawthorne and Cobb (1990). Models in which the VLBI core is taken to be a standing shock are considered, for example, by Cawthorne et al. (2013) and Marscher (2014) [see also references therein].

5.4.3 Faraday Rotation

Faraday rotation is a rotation of the plane of polarization of an electromagnetic (EM) wave that occurs when it passes through a region with free charges and magnetic field. Any EM wave can be described as the sum of any two orthogonal components, usually considered in radio astronomy to be right circularly polarized (RCP) and left circularly polarized (LCP). Due to asymmetry in the interactions between the local free charges and the RCP and LCP components of the polarized wave, these two components have different indices of refraction, and therefore different speeds of propagation through the magnetized medium.

When the wave propagates through a vacuum, the \mathbf{E} vectors for these two components rotate in opposite directions at the same rate, preserving the orientation of the plane of linear polarization, χ . When the wave propagates through a magnetized plasma, the difference in the speeds of the RCP and LCP waves induces a delay between these components, manifest as a rotation in the plane of polarization. The amount of rotation depends on the strength of the ambient magnetic field \mathbf{B} , the number density of charges in the plasma n_e , the charge e and mass m of these charges, and the wavelength of the radiation λ :

$$\chi = \chi_o + RM\lambda^2 \qquad RM = \frac{e^3}{8\pi^2\epsilon_o m^2 c^3} \int n_e \mathbf{B} \cdot d\mathbf{l} \qquad (5.10)$$

where χ is the observed polarization angle, χ_o is the intrinsic emitted polarization angle, and the integral is carried out over the line of sight from the source to the observer. Due to the inverse dependence on the square of the mass of the Faraday-rotating particles, it is usually assumed that observed Faraday rotation is due to the action of electrons; because the effective masses of relativistic electrons are higher than those of thermal electrons, these electrons are usually assumed to be thermal. The magnitude of the rotation measure RM depends on both n_e and the line-of-sight component of the magnetic field, while the sign of the Faraday rotation is determined by the direction of the line-of-sight magnetic field (either toward or away from the observer). The action of Faraday rotation can be identified through the λ^2 dependence of the observed polarization angle χ .

Note that it is the line-of-sight component of the ambient magnetic field that determines the magnitude and sign of the Faraday rotation. Essentially all observations of extragalactic sources are affected by Faraday rotation to some extent, because their radiation must always pass through our own Galaxy on its way to the Earth. Usually, these rotations are not very large at wavelengths of about 6 cm and shorter.

5.4.4 Faraday Depolarization

Faraday rotation can also give rise to *depolarization* of the radiation (e.g. Burn 1966). For example, if the source emission region is optically thin (little absorption of the radiation within the source), the radiation emitted at different depths in the source will pass through different amounts of the source volume on its way toward the observer. Therefore, if there are free electrons in the source volume, radiation emitted at different depths in the source will experience different amounts of Faraday rotation on its way through the source volume toward the observer. This causes a reduction in polarization, since it induces various offsets between emitted polarization electric vectors that are intrinsically aligned, essentially introducing a random component to the polarization. This is referred to as *front-back depolarization*.

Observations have some finite resolution, and so represent the sum of many electromagnetic waves propagating along many different lines of sight through the plasma. If appreciable inhomogeneities are present in the plasma electron density and/or ambient magnetic field on scales smaller than the resolution of the observations, different lines of sight will experience different rotation measures; this likewise leads to offsets between emitted polarization electric vectors that are intrinsically aligned, giving rise to *beam depolarization*.

Finally, if relatively large bandwidths are used at relatively long wavelengths, there can be appreciably different amounts of Faraday rotation occurring at the different frequencies in the observed band. If the signals detected within the band are averaged together, the observed polarization will be reduced, since intrinsically aligned polarization electric vectors at different frequencies within the band will

become offset due to the different Faraday rotations they experience; this is referred to as *bandwidth depolarization*.

In all cases, the depolarization occurs because the total polarization is the sum of the polarizations for multiple regions, lines of sight, or nearby frequencies that experience different Faraday rotations. Because the rotation of the polarization vectors is greater at longer wavelengths, such depolarization will also increase at longer wavelengths. Depolarization is indicated by a decrease in the observed degree of polarization with increasing wavelength.

5.4.5 Faraday Conversion

As was noted in Sect. 5.3.3, incoherent synchrotron radiation produces a only very small amount of circular polarization at frequencies of several to tens of gigahertz. Another mechanism that is capable of producing higher levels of circular polarization is the Faraday conversion of linear-to-circular polarization during propagation through a magnetized plasma (Jones and O'Dell 1977; Jones 1988).

Similar to Faraday rotation, Faraday conversion can occur when a polarized electromagnetic wave passes through a magnetized plasma. In order for Faraday conversion to operate, the observed linear polarization electric (\mathbf{E}) vector must have non-zero components both parallel to (\mathbf{E}_{\parallel}) and perpendicular to (\mathbf{E}_{\perp}) the magnetic field in the conversion region projected onto the sky, \mathbf{B}_{conv} . The electric-field component \mathbf{E}_{\parallel} excites oscillations of free charges in the plasma, while \mathbf{E}_{\perp} cannot, since the charges are not free to move perpendicular to \mathbf{B}_{conv} . This leads to a delay between \mathbf{E}_{\parallel} and \mathbf{E}_{\perp} , manifest as the introduction of a small amount of CP; the sign of the CP depends on the relative phase of \mathbf{E}_{\parallel} and \mathbf{E}_{\perp} .

Faraday conversion is a direct analog of Faraday rotation, but unlike Faraday rotation, Faraday conversion does not depend on the sign of the free charges involved. If the polarization \mathbf{E} vector is entirely parallel to the ambient magnetic field in the conversion region, it will be entirely absorbed and re-emitted, so that no delay, and hence no circular polarization, will be generated. Similarly, if \mathbf{E} is entirely orthogonal to the ambient magnetic field, it cannot be absorbed at all, so that again, no circular polarization will be generated.

5.5 What is Actually Observed?

5.5.1 Intensity Structures and Kinematics

Core-dominated AGN almost universally display one-sided core-jet structures on VLBI scales, consistent with a picture in which we are detecting only the Doppler-boosted approaching jet. Apparent superluminal motions are also extremely

common, again consistent with relativistic jets oriented at relatively small angles to the line of sight.

Although there is considerable overlap between the two distributions, it has long been known that different types of AGN display somewhat different typical superluminal speeds. On average, lower apparent speeds are observed in BL Lac objects, characterized by weak optical line emission, than in quasars, characterized by stronger optical line emission (Gabuzda et al. 1994, 2000; Kellermann et al. 2004). This systematic difference could in principle be associated with a difference in either the intrinsic flow speeds in the jet or the angles made by the jets to the line of sight. If due primarily to a difference in the characteristic viewing angles of the jets, the lower speeds observed in BL Lac objects would indicate that their jets are typically viewed at angles θ that are further from the angle $1/\Gamma$ that maximises the observed apparent speed than is the case for quasars, where Γ is the bulk Lorentz factor of the jet. BL Lac objects would be observed to have relatively low superluminal speeds if θ were either appreciably *larger* or appreciably *smaller* than $1/\Gamma$. The strong variability of BL Lac objects argues against the idea that their jets are typically viewed at relatively large angles to the line of sight. Further, Gabuzda et al. (2000) pointed out that the lack of evidence that BL Lac objects are typically more beamed than quasars argues against a scenario in which the jets of BL Lac objects are viewed at angles appreciably smaller than the viewing angles of quasar jets. Accordingly, Gabuzda et al. (2000) conclude that the lower apparent superluminal speeds of BL Lac objects most likely reflect lower average bulk Lorentz factors for their jets.

VLBI jets are frequently bent, although the origin of the observed bending is usually not clear (e.g. Kellermann et al. 1998b; Zensus et al. 2002). It must also be borne in mind that relatively small intrinsic bends can appear like much larger bends when projected onto the plane of the sky. Apparent bending need not imply non-ballistic motion of individual parcels of the jet plasma. For example, changes in the direction of ejection of the “nozzle” at the base of the jet could give rise to apparent bends in the jet, as in the well known stellar system SS433, whose jets are precessing (e.g. Blundell and Bowler 2004). Periodic outbursts or evidence for periodicity in changes in the ejection position angles have been reported for a number of AGN, which has been interpreted as evidence for precession (Stirling et al. 2003; Caproni and Abraham 2004a,b; Caproni et al. 2013; Klare et al. 2005; Qian et al. 2009).

Accelerations and non-radial motions of individual components have also been observed (e.g. Homan et al. 2003; Jorstad et al. 2004; Bloom et al. 2013). These can sometimes be difficult to interpret unambiguously, since we are observing the motions projected onto the plane of the sky, but they seem to indicate changes in both the speed and direction of motion of individual features.

Another behaviour that has recently been identified is “jet swinging” – a difficult to interpret phenomenon in which correlated non-radial component motions are observed (Agudo et al. 2007). This corresponds to a superluminal change in the overall position angle of the jet, as if the jet were acting like a rigid structure, possibly indicating an important role of the magnetic field in the jet dynamics.

Stationary or nearly stationary features that have been interpreted as standing shocks have also been observed in a number of sources. These are sometimes close to the core (e.g. BL Lac: Cohen et al. 2014) and sometimes at an appreciable distance from the core (e.g. 1803+784: Britzen et al. 2005). Cohen et al. (2014) have suggested that a quasi-stationary feature observed at 15 GHz only 0.26 mas from the core is a recollimation shock, and that components emanating from this feature represent compressions established by slow and fast mode magneto-acoustic MHD waves propagating in a region of toroidal \mathbf{B} field.

A problem that is continually encountered in the interpretation of multi-epoch VLBI images is disentangling the intrinsic speed of the flow from the viewing angle, as in Eq. (5.3) for the observed superluminal motions. One approach is to estimate the Doppler factor (Eq. (5.6)) based on observations of source variability and use this together with observed superluminal speeds to derive estimates of the jet speeds and jet viewing angles (Hovatta et al. 2009). Fitting of transverse polarization profiles using a helical-field model, as has been carried out by Murphy et al. (2013), can be used to estimate the viewing angle of the jet in the jet rest frame, which can then be used with measured superluminal speeds and the aberration formulas (5.1) to derive estimates of the intrinsic jet speeds and jet viewing angles in the observer's frame. Such an analysis for Mrk501 yielded the intrinsic jet speed $\beta = 0.96$ and viewing angle in the observer's frame $\theta = 15^\circ$, consistent with but more constraining than the earlier results of Giroletti et al. (2004) [$\beta \geq 0.88$, $\theta \leq 27^\circ$]. Transverse profile fitting for 3C 273 (Gabuzda et al., in prep) yielded $\Gamma = 13.6$ and $\theta = 3.8^\circ$, in excellent agreement with the estimates of Hovatta et al. (2009) based on their variability analysis, $\Gamma = 14$ and $\theta = 4^\circ$. Cross-checking estimates obtained using these two approaches for additional AGNs can potentially provide important verification of the reliability of such estimates.

5.5.2 Magnetic-Field Structures

The observed degrees of polarization in the jets of AGN range from a few percent up to 50–60%, fully consistent with the jet emission being incoherent synchrotron radiation in a partially ordered \mathbf{B} field. In most cases, the observed polarization vectors – and therefore the associated jet \mathbf{B} fields – in the VLBI jets of AGN tend to be either parallel or perpendicular to the local jet direction. This should come about naturally if the jets locally exhibit approximately cylindrical symmetry: the \mathbf{B} field can always be separated into longitudinal and transverse components projected onto the sky (e.g. Lyutikov et al. 2005).

Various polarization patterns are fairly commonly, illustrated schematically in Fig. 5.4, which shows an intensity image taken from the website of the MOJAVE project (see the Acknowledgements) with artificial polarization sticks superimposed (recall that the observed polarization is orthogonal to the underlying \mathbf{B} field in optically thin regions, such as the jet). Possible origins for each of these patterns are considered below.

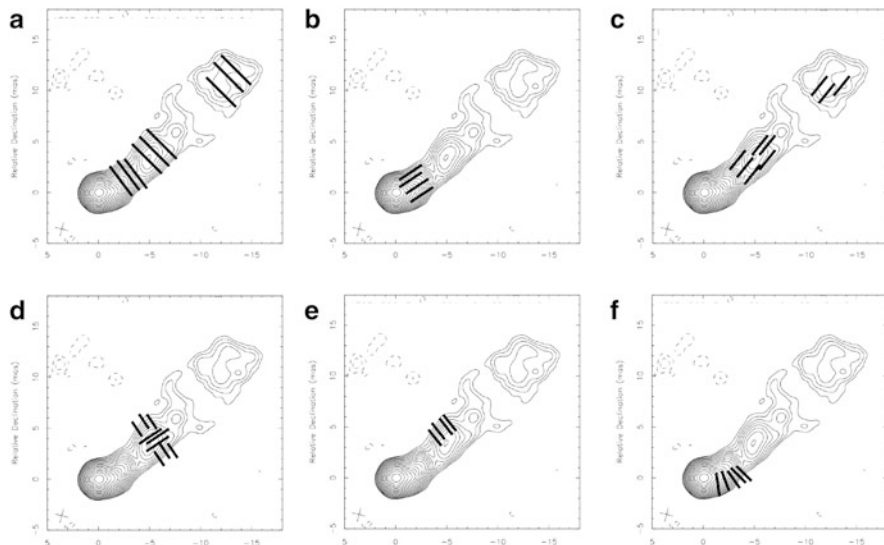


Fig. 5.4 Schematics of various polarization patterns commonly observed in AGN jets, corresponding to: (a) extended regions of longitudinal field; (b) regions of orthogonal field associated with bright, compact regions; (c) extended regions of orthogonal field; (d) spine–sheath transverse \mathbf{B} -field structure; (e) longitudinal field offset toward one side of the jet; (f) longitudinal field around a bend in the jet. Recall that the \mathbf{B} field is orthogonal to the observed polarization in optically thin regions. The contour map was taken from the MOJAVE website (see the Acknowledgements), and the sticks added to illustrate the various polarization configurations

Extended regions with longitudinal \mathbf{B} field, as in Fig. 5.4a, could come about due to shear with the surrounding medium stretching out the magnetic field along the flow and thereby enhancing the longitudinal component. Alternatively, such regions could be associated with a helical \mathbf{B} field with a comparatively low pitch angle (the angle between the \mathbf{B} field lines and the jet axis); i.e., a “loosely wound” helical field.

Compact features with orthogonal \mathbf{B} field, as in Fig. 5.4b, are candidates for regions of transverse shocks (Laing 1980; Hughes et al. 1985). In a region subject to shock compression, the \mathbf{B} field is amplified in the plane of compression, giving rise to appreciable degrees of polarization and a net magnetic field lying in the plane of compression, even in the case of an initially completely tangled magnetic field.

Extended regions of orthogonal \mathbf{B} field, as in Fig. 5.4c, could in principle be due to a series of transverse shocks, but this picture seems somewhat contrived. It is probably more likely that such regions are revealing the presence of a toroidal field or high-pitch-angle (“tightly wound”) helical field.

Spine–sheath polarization structure implying an orthogonal \mathbf{B} field near the jet ridgeline and longitudinal \mathbf{B} field near one or both edges of the jet (Fig. 5.4d) could reflect the joint action of shock compression and a shear interaction with the surrounding medium (as proposed, e.g. by Attridge et al. 1999). However, this type of \mathbf{B} -field structure could also be associated with a helical field in which the

azimuthal component dominates near the center of the jet and the longitudinal component dominates near the jet edges, projected onto the sky (e.g. Pushkarev et al. 2005; Lyutikov et al. 2005). In the latter case, this should also give rise to an increase in the degree of polarization toward the jet edges.

Longitudinal \mathbf{B} field offset from the jet ridgeline (Fig. 5.4e) could be associated with either a shear interaction occurring on one side of the jet or a helical \mathbf{B} field. Some combinations of pitch angle and viewing angle should give rise to projected helical \mathbf{B} -field configurations with longitudinal field on one side of the jet and transverse field on the other, which may be observed simply as an offset longitudinal field if the transverse field has much weaker polarization (e.g. Murphy et al. 2013).

Longitudinal \mathbf{B} field along a bend in the jet (Fig. 5.4f) could be due to a shear interaction with the surrounding medium, or alternately to an enhancement (“stretching out”) of the longitudinal component of the field due to the bending of the jet, sometimes referred to a “curvature-induced polarization”.

More rarely, the observed polarization does not show an obvious relationship to the jet direction, even when the polarization angles have been corrected for Faraday rotation or the observations are at a high enough frequency that Faraday rotation is unlikely to be appreciable (examples can be found among the sources monitored by the MOJAVE project, e.g., Lister and Homan 2005). The origin of such “offset” polarization angles (\mathbf{B} fields) is not clear, although one possibility may be oblique shocks or inaccurate knowledge of the local jet direction due to limited resolution. Intriguing fan-like structures have also been observed, which may represent conical shocks (e.g. Papageorgiou et al. 2006).

As is clear from the list above, the origin of the implied \mathbf{B} -field structure is usually not clear from the observed polarization-angle distribution alone, and additional information is usually required as the basis for interpretation, such as the distribution of the degree of polarization, information about Faraday rotation occurring in the vicinity of the AGN etc.

5.5.3 Core Polarization

The core components are typically polarized from less than 1% to a few percent, consistent with the emission being incoherent synchrotron radiation in a partially ordered \mathbf{B} field; the spectral indices at centimeter wavelengths are typically fairly flat, indicating that this region is at least partially optically thick. In most cases, the observed polarization vectors at relatively short centimeter wavelengths tend to be either parallel or perpendicular to the direction of the inner jet, although offsets due to appreciable Faraday rotation can sometimes affect the observed core polarization directions at longer centimeter wavelengths. Whether these imply \mathbf{B} fields that are aligned with or orthogonal to the jet direction depends on whether the net core polarization is predominantly from regions that are optically thin (χ perpendicular to \mathbf{B}) or optically thick (χ parallel to \mathbf{B}).

There is good evidence that the observed core polarizations are associated with predominantly optically thin regions in many cases. The observed core polarizations are typically a few percent, and can reach as high as 10% (e.g. Lister and Homan 2005); this would require fairly highly ordered \mathbf{B} fields in the core region if this was associated with optically thick regions capable of generating a maximum degree of polarization of 10–12%. The orientation of the core and inner jet polarization angles is often the same, consistent with a picture in which they are both associated with predominantly optically thin regions with the same \mathbf{B} field configuration on different scales (e.g. Lister and Homan 2005). In addition, the Faraday-corrected core polarization angles of a number of BL Lac objects were found to be well aligned with nearly simultaneously measured optical polarization angles, suggesting roughly co-spatial optically thin emission regions in both wavebands (Gabuzda et al. 2006).

It is an interesting question how to relate the observed VLBI cores to the theoretical concept of the core as the $\tau = 1$ surface in a Blandford–Königl jet (Blandford and Königl 1979). As is argued in the previous paragraph, there is considerable evidence that the core polarization is associated predominantly with optically thin emission. The core spectral indices α ($S_\nu \propto \nu^{+\alpha}$) are usually fairly flat, between -0.5 and $+0.5$, (e.g. Hovatta et al. 2014), with the vast majority of the most positive spectral indices extending up to $+1$, consistent with the idea that the observed cores include a mixture of optically thick and optically thin regions. Gabuzda and Gómez (2001) have reported a rotation of the observed core polarization angle in OJ287 by roughly 90° between 5 and 15 GHz, which they interpreted as an optically thick–thin transition; i.e., the observed core polarization was emitted by a region that was predominantly optically thin at 15 GHz but predominantly optically thick at 5 GHz. All this suggests that what we observe as the VLBI core represents a region that is only partially optically thick, corresponding to a mixture of the optically thick base of the jet (as in the Blandford–Königl picture) and optically thin regions in the innermost jet, with the latter often dominating the observed core polarization.

An alternate view of the VLBI core is that it represents a standing or recollimation shock. Gabuzda et al. (2013) are able to describe the fan-like polarization observed in the VLBI core of 1803+784 as a conical recollimation shock. Marscher (2014) (see also references therein) has recently developed a model for the variability of the flux and polarization of compact AGN in which turbulent plasma flowing at a relativistic speed down a jet crosses a standing conical shock, which we observe as the VLBI core.

5.5.4 Core Shifts and Core Magnetic Fields

The first study aimed at using the frequency dependence of AGN VLBI-core positions to estimate the core B-field strengths were carried out by Lobanov (1998). Based on images at only three frequencies, this analysis showed that the position

of the VLBI core seemed to show the expected sort of frequency dependence, but only limited conclusions could be drawn, due to the limited number of frequencies and sources considered. Nevertheless, this work was important, as it laid out an approach to estimating the core B fields based on measurement of the core position as a function of frequency.

After an interval of more than a decade, there has recently been an explosion of new core-shift studies, most notably those of Kovalev et al. (2008), O’Sullivan and Gabuzda (2009), Sokolovsky et al. (2011) and Pushkarev et al. (2012). O’Sullivan and Gabuzda (2009) were the first to carry out a core-shift analysis for VLBI observations obtained simultaneously at more than only two to three frequencies. Their data based on eight frequencies from 4.6 to 43 GHz provided detailed and redundant measurements, which clearly demonstrated the expected power-law dependence of the core position as a function of frequency. These measurements also provided evidence that the parameter $k_r \simeq 1$ in most of the six AGN considered, where the position of the VLBI core r as a function of frequency ν is given by $r \propto \nu^{-1/k_r}$; a reasonable interpretation of the result that $k_r \simeq 1$ is that these core regions are close to equipartition, with the magnetic field $B \sim r^{-1}$ and the electron density $N \sim r^{-2}$. This is potentially a very important result, since equipartition has often assumed for various calculations, but without any observational evidence that this assumption is reasonable. Kovalev et al. (2008) were the first to derive core-shift measurements for a much larger number of sources (29), but at only two frequencies, while Sokolovsky et al. (2011) obtained results for 20 sources at nine frequencies. Most recently, Pushkarev et al. (2012) obtained core-shift data for more than a hundred well-studied sources from the MOJAVE project (web page) at four frequencies from 8.1 to 15.4 GHz. The core-region B fields inferred from these studies are generally tenths of a Gauss; Pushkarev et al. (2012) found evidence that the core B fields of quasars are somewhat higher than those in BL Lac objects, which is presumably related to the higher luminosities of quasars in some way.

5.5.5 *Circular Polarization*

Techniques for deriving circular-polarization (CP) information on parsec scales were pioneered by Homan and his collaborators in the late 1990s (Homan and Wardle 1999; Homan et al. 2001) using data taken on the VLBA. CP measurements for the first epoch of the MOJAVE project (monitoring of 133 AGN at 15 GHz with the VLBA) were published by Homan and Lister (2006). Circular polarization was detected in 34 of these objects at the 2σ level or higher. These results confirmed previously noted trends: the circular polarization is nearly always coincident with the VLBI core, with typical degrees of polarization m_c being a few tenths of a percent. Homan and Lister (2006) found no evidence for any correlation between m_c and

any of 20 different optical, radio and intrinsic parameters of the AGN. Interestingly, five of the 34 AGN displayed CP in their *jets*, well outside the VLBI-core region, suggesting that the mechanism generating the circular polarization is capable of operating effectively in optically thin regions.

The two main mechanisms that are usually considered to be the most likely generators of the observed CP are the synchrotron mechanism and the Faraday conversion of linear to circular polarization, as described in Sect. 5.3.3. Although the intrinsic CP generated by synchrotron radiation may be able to reach a few tenths of a percent at 15 GHz for the \mathbf{B} -field strengths characteristic of the observed VLBI cores of AGN (Sect. 5.5.3), the highest observed m_c values seem too high to plausibly be attributed to this mechanism. This suggests that Faraday conversion plays a significant, and possibly dominant role, since it is expected to be more efficient at generating CP than the synchrotron mechanism for the conditions in radio cores (Jones and O’Dell 1977).

Few multi-frequency CP measurements have been published, and relatively little is currently known about the frequency dependence of the observed CP. The 15+22+43-GHz results of Vitrishchak et al. (2008) showed excellent agreement with the earlier 15-GHz measurements of Homan and Lister (2006). They did not show any universal frequency dependence for m_c , with both rising and falling spectra with frequency being observed; similarly, Homan and Wardle (2004) found very different spectral indices for the degree of CP, α_c ($|m_c| \propto \nu^{\alpha_c}$), for three CP components in the inner jet of the nearby ($z = 0.017$) radio galaxy 3C84: $\alpha_c = -0.9$ for a component with positive CP in a predominantly optically thin region and $\alpha_c = +1.4$ and $+1.7$ for two components with negative CP in partially optically thick regions. Vitrishchak et al. (2008) found m_c to be higher at 43 GHz than at their lower two frequencies. These results seem contrary to expectations, since the degree of circular polarization from both synchrotron radiation and Faraday conversion should decrease towards higher frequencies if the source is homogeneous. Vitrishchak et al. (2008) also found evidence in several objects that the detected circular polarization was near, but not coincident with the core, as well as several cases of changes in sign with frequency.

The collected VLBI-scale circular-polarization measurements indicate that the sign of the circular polarization at a given observing frequency is generally consistent across epochs separated by several years or more, suggesting stability of the magnetic field orientation in the innermost jets. Overall, it seems likely that the observed CP is predominantly generated by Faraday conversion, and that the observed values of α_c are determined by effects associated with the intrinsic inhomogeneity of the jets, as well as the possible presence of several regions of CP of either one or both signs contributing to the observed “core” CP (see the discussion in Vitrishchak et al. 2008 and Wardle and Homan 2003).

5.5.6 Parsec-Scale Faraday Rotation Measurements

Core vs. jet rotation measures A number of early Faraday-rotation studies of AGN on parsec scales were carried out by Taylor (1998, 2000) and Zavala and Taylor (2003, 2004), who were primarily interested in looking for differences between the core and jet RM values. These Faraday-rotation maps for about 40 AGN showed a clear tendency for the core RMs to be greater in magnitude than the jet RMs, apparently due to higher electron densities and magnetic-field strengths on smaller scales in the jets. These studies also presented evidence that the core RMs of quasars tend to be higher than those of BL Lac objects; it is an obvious possibility that this is related to the stronger optical line emission of quasars, compared to BL Lac objects.

Faraday rotation as a probe of the azimuthal \mathbf{B} field As was pointed out by Blandford (1993), if a jet has a helical \mathbf{B} field, we should observe a Faraday-rotation gradient across the jet, due to the systematically changing line-of-sight component of the \mathbf{B} field across the jet. Thus, the detection of transverse Faraday-rotation gradients across AGN jets could potentially provide a powerful diagnostic for the presence of an azimuthal field component associated with a helical or toroidal jet \mathbf{B} field. The theoretical simulations of Broderick and McKinney (2010) directly demonstrate the development of helical jet \mathbf{B} fields and the resulting presence of Faraday rotation gradients across the simulated jets.

A number of transverse Faraday-rotation gradients across AGN jets have been reported in the literature, most recently by Asada et al. (2010), Croke et al. (2010), Gómez et al. (2011), Hovatta et al. (2012), Mahmud et al. (2013) and Gabuzda et al. (2013, 2014); an example is shown in Fig. 5.5. Gómez et al. (2011) superposed

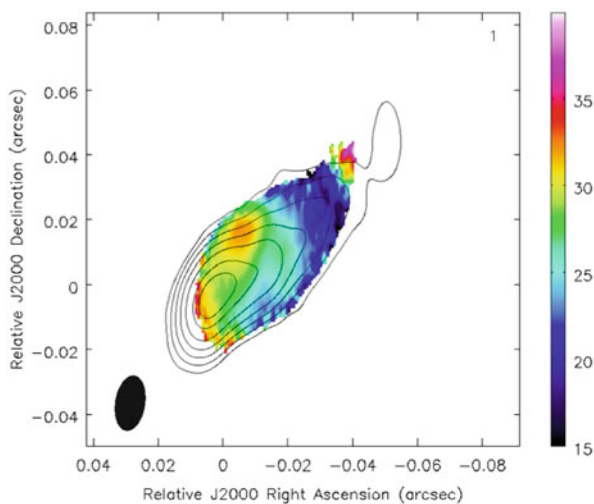


Fig. 5.5 Transverse Faraday RM gradient across the VLBI jet of 3C380 (Gabuzda et al. 2013)

degree of polarization and RM images for 3C120 obtained at multiple epochs to effectively map out these quantities along a much longer portion of the jet than was possible at any single epoch, making the transverse structure in the polarization and Faraday rotation appreciably clearer.

Of course, it is also possible to imagine situations when a gradient in the Faraday rotation roughly across a VLBI jet occurs, not due to a systematic variation in the line-of-sight \mathbf{B} -field component, but due to a gradient in the density of thermal electrons in the region surrounding the jet. This could be the case, for example, if the jet were propagating through a non-uniform medium that was denser on one side of the jet than on the other. In this regard, it is important to point out a crucial discriminator: while transverse RM gradients with RM values of a single sign that increase toward one edge of the jet could potentially be caused by either a helical jet \mathbf{B} field or a density gradient in the surrounding medium, transverse RM gradients that display one sign at one edge of the jet, pass through zero and then display the other sign at the other edge of the jet are a clear and unambiguous sign of a helical jet \mathbf{B} field. It is therefore highly significant that transverse RM gradients displaying *both* signs have been observed for a number of AGN, after subtracting the effect of the RM arising in our Galaxy; in such cases, the only plausible explanation for the observed transverse RM gradients is that the corresponding jets have helical \mathbf{B} fields.

As Sikora et al. (2005) have pointed out, the lack of deviations from a λ^2 wavelength dependence for the observed polarization angles in some case indicates that the Faraday rotation must be external, suggesting that the associated helical \mathbf{B} field may surround the jet, but not necessarily fill the jet volume; alternatively, it may be that the helical field fills the jet volume, but the thermal electrons required for the Faraday rotation do not.

Reliability of observed Faraday-rotation gradients Thus, a number of studies carried out in different groups around the world have reported detections of transverse Faraday-rotation gradients across AGN jets on parsec scales, interpreted as evidence for helical jet \mathbf{B} fields. Further, the theoretical simulations of the propagation of jets from a rotating black hole/accretion disk system carried out by Broderick and McKinney (2010) clearly showed the presence of transverse RM gradients, including across the VLBI core regions, and also showed that these could sometimes remain visible even when convolved with a beam that was much larger than the intrinsic jet width (e.g. a 0.9-mas beam and an intrinsic jet width at its base of about 0.05 mas; Fig. 8 in Broderick and McKinney 2010).

At the same time, it seems somewhat counter-intuitive that it could be possible to detect transverse polarization and Faraday rotation structure across poorly resolved jets, whose intrinsic widths may be much narrower than the beam. This led Taylor and Zavala (2010) to suggest that an observed Faraday-rotation gradients should span at least three “resolution elements” (usually taken to mean three beamwidths) across the jet in order to be considered reliable, although they did not present any demonstration that this was the case. In addition, there had been no clear agreement in early analyses of transverse Faraday-rotation gradients about the most correct way

to estimate the uncertainties on the RM values at specified locations in an RM image. Thus, there was a need to clarify whether there was a minimum resolution required to reliably detect Faraday-rotation structure, and identify a suitable approach for estimating uncertainties in quantities at individual locations in VLBI images.

A first important step was taken by Hovatta et al. (2012), who carried out Monte Carlo simulations based on realistic “snapshot” baseline coverage for VLBA observations at 7.9, 8.4, 12.9 and 15.4 GHz aimed at investigating the statistical occurrence of spurious RM gradients across jets with intrinsically constant polarization profiles. Inspection of the right-hand panel of Fig. 30 of Hovatta et al. (2012) shows that the fraction of spurious 3σ gradients was no more than about 1%, even for the smallest observed RM-gradient widths they considered, about 1.4 beamwidths. Relatively few 2σ gradients were also found, although this number reached about 7% for observed jet widths of about 1.5 beamwidths; nevertheless, Hovatta et al. (2012) point out that 2σ gradients are potentially also of interest if confirmed over two or more epochs. The results of Hovatta et al. (2012) have also now been confirmed by similar Monte Carlo simulations carried out by Algaba (2013) for simulated data at 12, 15 and 22 GHz and by Murphy and Gabuzda (2013) for simulated data at 1.38, 1.43, 1.49 and 1.67 GHz and at the same frequencies as those considered by Hovatta et al. (2012). The 1.38–1.67 GHz frequency range considered by Murphy and Gabuzda (2013) yielded a negligible number of spurious 3σ gradients and fewer than 1% spurious 2σ gradients, even for observed jet widths of only 1 beamwidth (i.e., for poorly resolved jets).

Two more sets of Monte Carlo simulations based on realistic snapshot VLBA baseline coverage adopted a complementary approach: instead of considering the occurrence of spurious RM gradients across jets with constant polarization, they considered simulated jets with various widths and with transverse RM gradients of various strengths, convolved with various size beams. Mahmud et al. (2013) carried out such simulations for 4.6, 5.0, 7.9, 8.4, 12.9 and 15.4 GHz VLBA data, and Murphy and Gabuzda (2013) for 1.38, 1.43, 1.49 and 1.67 GHz VLBA data. These simulations clearly showed that, with realistic noise and baseline coverage, the simulated RM gradients could remain clearly visible, even when the jet width was as small as 1/20 of a beam width.

All these simulations clearly demonstrate that the width spanned by an RM gradient is not a crucial criterion for its reliability.

Another key outcome of the Monte Carlo simulations of Hovatta et al. (2012) is an empirical formula that can be used to estimate the uncertainties in intensity (Stokes I , Q or U) images, including the uncertainty due to residual instrumental polarization (“D-terms”) that has been incompletely removed from the visibility data. In regions of source emission where the contribution of the residual instrumental polarization is negligible, the typical uncertainties in individual pixels are approximately 1.8 times the rms deviations of the flux about its mean value far from regions of source emission. This is roughly a factor of two greater than

the uncertainties that have usually been assigned to the intensities measured in individual pixels in past studies, indicating that the past uncertainties have been somewhat underestimated. These results have recently been confirmed by the Monte Carlo simulations of Coughlan (2014), which likewise indicate that the typical intensity uncertainties in individual pixels are of order twice the off-source rms, with significant pixel-to-pixel variations in the uncertainties appearing in the case of well resolved sources.

The reliability of transverse RM gradients observed across the partially optically thick core regions remains an open question, and further simulations are required to investigate this in more detail. However, since (as is argued in Sect. 5.5.3) what we observe as the “VLBI core” with beamwidths of the order of a milliarcsecond is actually a blend of the optically thick base of the jet and unresolved optically thin regions in the innermost jet, it is likely that the polarization of the observed core components is dominated by optically thin emission in many cases. In addition, the theoretical simulations of Broderick and McKinney (2010) show smooth, monotonic RM gradients across the VLBI core regions when they are convolved with a 0.9-mas beam. This all suggests that transverse RM gradients across core regions may often be reliable, but further simulations are required to test this more directly.

Evidence for the return \mathbf{B} -field Mahmud et al. (2009, 2013) and Gabuzda et al. (2014) have reported reversals in the directions of observed transverse Faraday rotation gradients, either with distance along the jet (four AGNs) or with time (two AGNs).

These results at first seem puzzling, since the direction of a transverse RM gradient associated with a helical \mathbf{B} field is essentially determined by the direction of rotation of the central black hole and accretion disk and the initial direction of the poloidal field component that is “wound up” by the rotation. It is difficult in this simplest picture to imagine how the direction of the resulting azimuthal field component could change with distance along the jet or with time. However, in a picture with a nested helical field structure, similar to the “magnetic tower” model of Lynden–Bell (1996), but with the direction of the azimuthal field component being different in the inner and outer regions of helical field, such a change in the direction of the net observed RM gradient could be due to a change in dominance from the inner to the and outer region of helical field in terms of their overall contribution to the Faraday rotation (Mahmud et al. 2013).

Thus, the detection of such reversals in the directions of transverse RM gradients may provide the first observational evidence for the presence of the return \mathbf{B} field.

One theoretical picture that predicts a nested helical-field structure with oppositely directed azimuthal field components in the inner and outer regions of helical field is the “Poynting–Robertson cosmic battery” model of Contopoulos et al. (2009) discussed in the following subsection, although other plausible systems of currents may also give rise to similar field configurations.

Evidence for a Cosmic Battery? Any transverse Faraday-rotation gradient can be described as being directed either clockwise (CW) or counter-clockwise (CCW) on the sky, relative to the base of the jet. Contopoulos et al. (2009) reported evidence for a significant excess of CW transverse Faraday-rotation gradients for parsec-scale AGN jets, based on transverse Faraday-rotation gradients identified in maps from the literature. This is an extremely counterintuitive result, since the direction of the helical field threading an AGN jet should essentially be determined by the direction of rotation of the central black hole and accretion disc, together with the direction of the poloidal “seed” field that is wound up, and our instincts tell us that both of these should be random. A re-analysis of the transverse Faraday-rotation gradients considered by Contopoulos et al. (2009) to verify their reliability applying the new error-estimation procedure of Hovatta et al. (2012) is currently underway (Gabuzda et al. 2014), but it appears that the reported asymmetry in the collected data will probably be confirmed.

Contopoulos et al. (2009) suggest that this non-intuitive result can be explained in a straightforward way via the action of a mechanism they call the “Poynting–Robertson cosmic battery.” The essence of this mechanism is the Poynting–Robertson drag experienced by charges in the accretion disc, which absorb energy emitted by the active nucleus and re-radiate this energy isotropically in their own rest frames. Because these charges are rotating with the accretion disc, this radiation will be beamed in the forward direction of their motion, i.e., in the direction of the disc rotation. Due to conservation of momentum, the charges then feel a reaction force opposite to the direction of their motion; since the magnitude of this force exhibits an inverse dependence on the mass of the charge, this leads to a difference in the deceleration experienced by the protons and electrons in the disc. Since the electrons are decelerated more strongly, this leads to a net current in the disc, in the direction of rotation. This current, in turn, gives rise to a net poloidal magnetic field whose direction is coupled to the direction of the current in the disc, i.e., to the direction of the disc rotation. This coupling of the disc rotation and the direction of the poloidal field that is “wound up” breaks the symmetry in the direction of the toroidal field component, and predicts that the observed Faraday-rotation gradients should be predominantly CW on the sky, independent of the direction of the disc rotation as seen by the observer. In a “nested helical field” type picture such as that described in the previous subsection, the inner/outer regions of helical field should give rise to CW/CCW Faraday-rotation gradients; therefore, the observed excess of CW implies that the inner region of helical \mathbf{B} field dominates on parsec scales.

If this excess of CW Faraday-rotation gradients is indeed confirmed by further studies, this will have cardinal implications for our understanding of AGN jets. If the Poynting–Robertson battery does not operate sufficiently efficiently to provide the observed excess of CW gradients, then some other mechanism generating a suitable system of \mathbf{B} fields and currents must be identified.

5.5.7 *Helical Jet Magnetic Fields: Basis for a New Paradigm?*

From a theoretical point of view, it would be very natural if many, or possibly even all, AGN jets are associated with helical \mathbf{B} fields, produced essentially by the “winding up” of an initial “seed” field threading the accretion disc by the combination of the rotation of the central black hole and accretion disc and the jet outflow (e.g. Nakamura et al. 2001; Meier et al. 2001; Lovelace et al. 2002; Lynden–Bell 2003; Tsinganos and Bogovalov 2002). The possibility that toroidal field components develop in association with currents flowing in the jet has also been considered (Pariiev et al. 2003; Lyutikov 2003). Indeed, these two ideas are not unrelated: whether or not it is related to a helical \mathbf{B} field, if there is a dominant toroidal \mathbf{B} -field component, basic physics tells us that there must be currents flowing in the region enclosed by the field.

This very plausible theoretical picture provides strong motivation to consider interpretations of observed properties of AGN jets as possible consequences of helical/toroidal \mathbf{B} -field structures. The role of transverse Faraday rotation gradients in revealing the presence of a toroidal or helical \mathbf{B} field has already been discussed; several other pieces of observational evidence supporting the idea that many AGN jets carry helical \mathbf{B} fields are considered below.

B-field configurations In general, a helical \mathbf{B} field can be described as a superposition of a toroidal (azimuthal) and a longitudinal component. The larger the pitch angle (angle between the helix axis (jet axis) and \mathbf{B} vector), i.e. the more tightly wound the helix, the stronger the toroidal relative to the longitudinal component. Depending on the combination of the pitch angle and viewing angle, an overall helical jet \mathbf{B} field can give rise to an observed field structure that is everywhere orthogonal, everywhere longitudinal, orthogonal and longitudinal on either side of the jet, or spine–sheath-like, with a region of orthogonal field near the jet axis flanked on one or both sides with regions of longitudinal field. Thus, many of the polarization patterns observed for AGN jets can be understood as consequences of helical jet \mathbf{B} fields with various combinations of helical pitch angles and viewing angles.

Transverse B-field structure The best case for polarization configurations best explained by helical jet \mathbf{B} fields are asymmetric transverse structures, such as spine–sheath polarization structures or longitudinal polarization that is not centered on the jet ridgeline. When an AGN also displays a transverse Faraday-rotation gradient, consistency between the properties of this gradient and the observed transverse polarization structure can be checked. Here, we must recall that the degree of polarization is determined by the component of the jet \mathbf{B} field in the plane of the sky (e.g., a \mathbf{B} field directed precisely toward the observer would give no linear polarization). As is shown by the helix in Fig. 5.6, the poloidal component of a helical field projected onto the sky makes the overall field lie predominantly along

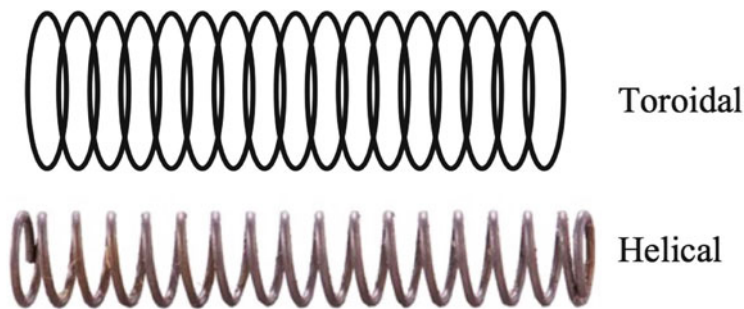


Fig. 5.6 Schematic illustrating how a toroidal jet \mathbf{B} -field geometry should give rise to symmetrical polarization structure across the jet, while a helical jet \mathbf{B} -field geometry should give rise to an asymmetrical transverse polarization structure

the line of sight at one edge of the helix, giving rise to higher Faraday rotation and lower degrees of polarization (top edge of the helix shown), and predominantly in the plane of the sky at the other edge of the helix, giving rise to lower Faraday rotation and higher degrees of polarization (bottom edge of the helix shown).

Murphy et al. (2013) have recently carried out fitting of the transverse total intensity and polarization profile across the jet of Mrk501 on parsec scales, which display appreciable asymmetry. The profiles were fit well using a simple helical-field model with a pitch angle of about 53° and a viewing angle in the jet rest frame of about 83° (recall that this corresponds to a much smaller viewing angle in the observer’s frame due to aberration). In addition, the parsec-scale jet of Mrk501 exhibits a transverse RM gradient (Gabuzda et al. 2004; Croke et al. 2010), with the larger-magnitude RM values present on the side of the jet with a lower degree of polarization, as is expected for a helical jet \mathbf{B} field. Although such results are available for only one or two sources, this approach could potentially be quite valuable when applied to a larger number of AGN of different types. Profile fitting can also be used to investigate change in the pitch angle and viewing angle of the helical field along the jet.

Circular polarization As is indicated above, it is generally agreed that the most plausible mechanism for the generation of the circular polarization observed on VLBI scales in AGN is the Faraday conversion of linear-to-circular polarization during the propagation of a linearly polarized electromagnetic wave through a magnetized plasma (Jones and O’Dell 1977; Jones 1988). In order for Faraday conversion to operate, the \mathbf{B} field in the conversion region \mathbf{B}_{conv} must have a non-zero component parallel to the plane of linear polarization. For this reason, as has been pointed out by Wardle and Homan (2001), a helical \mathbf{B} field provides an interesting example of an overall ordered \mathbf{B} field geometry that can potentially facilitate linear-to-circular conversion: synchrotron radiation emitted at the “far” side of the helical field relative to the observer can undergo conversion in the “near” side of the helical field. This raises the question of whether the CP detected in

AGN on VLBI scales could be generated in helical **B** fields associated with the corresponding AGN jets. Inspection of the MOJAVE sources in which CP was detected (Homan and Lister 2006) reveals that a number of them show various properties that can be associated with the presence of helical jet **B** fields, such as extended regions of transverse **B** field, spine+sheath jet **B**-field structures and transverse RM gradients, providing indirect evidence that at least some of the detected CP may be associated with helical jet **B** fields. It is also intriguing that extended regions of CP clearly in the VLBI jet, well away from the optically thick core region, have now been detected in several cases (Homan and Lister 2006; Vitriřchak and Gabuzda 2007) – linear to circular conversion in helical **B** fields associated with these jets could explain this result in a natural way.

“Inverse depolarization” A surprising result to come out of an analysis of multi-wavelength data for the MOJAVE AGN sample was the identification of a number of AGN with components displaying degrees of polarization that increase with increasing wavelength (Hovatta et al. 2012). This is counter to the usual expectation that depolarization should correspond to decreasing polarization with increasing wavelength, and has accordingly been referred to as “inverse depolarization.” Homan (2012) has developed a model that can explain this unexpected behaviour as an effect of internal Faraday rotation occurring in a jet whose **B** field displays structural inhomogeneities, such as are naturally produced in helical jet **B** fields.

Superluminal speeds trends It has independently been suggested by Gabuzda et al. (2000) and Asada et al. (2002) that the observed difference in the typical superluminal speeds of BL Lac objects and quasars referred to in Sect. 5.5.1 could be related to another systematic difference in the VLBI properties of these two types of AGN: the VLBI jets of BL Lac objects/quasars most often display predominantly **B** fields that are orthogonal to/aligned with the jet direction. Let us suppose that both quasars and BL Lac objects characteristically have helical jet **B** fields that come about due to the combination of rotation of the central black hole/accretion disc and the jet outflow. If the intrinsic outflow speeds of quasars are, on average, higher than those of BL Lac objects, this might mean that the ratios of their outflow speeds to their central rotational speeds are also higher, giving rise to helical jet **B** fields that are less tightly wound. On the other hand, lower outflow speeds in BL Lac objects might lead to the helical **B** fields associated with their jets being more tightly wound. Thus, it may be possible to understand the observed systematic differences in the VLBI properties of BL Lac objects and quasars within a single scenario in which a tendency for lower outflow speeds in BL Lac objects compared to quasars leads to a tendency for more tightly wound helical jet **B** fields in BL Lac objects, which are manifest as a predominance for jet **B** fields orthogonal to the jet direction in these sources.

Can we distinguish between helical and toroidal fields? The detection of a transverse Faraday-rotation gradient across an AGN jet can reflect the presence of an azimuthal field component, but this component could be associated with either a helical or a toroidal **B** field. Generally speaking, it is only asymmetry of the intensity

and polarization profiles across the jet that can distinguish observationally between a helical field (with an ordered poloidal field component) and a toroidal field (with a disordered poloidal field component). Here, we must recall that the degree of polarization is determined by the component of the jet magnetic field in the plane of the sky (e.g., a magnetic field directed precisely toward the observer would give no linear polarization). Figure 5.6 shows qualitatively an example in which the poloidal field component of a helical field makes the overall field predominantly along the line of sight at one edge of the helix (giving rise to higher Faraday rotation and lower degrees of polarization), and predominantly in the plane of the sky at the other edge of the helix (giving rise to lower Faraday rotation and higher degrees of polarization). In contrast, in the absence of other factors, a toroidal field should give rise to a symmetric polarization profile across the jet, independent of the viewing.

Thus, the firm detection of asymmetric transverse polarization structure with a configuration consistent with one of those expected for helical fields provides a good diagnostic for the presence of a helical, as opposed to toroidal, **B** field.

Acknowledgements This review has made use of data from the MOJAVE database that is maintained by the MOJAVE team (Lister et al., 2009, *AJ*, 137, 3718). The image used to compose Fig. 5.4 was taken from the MOJAVE website, <http://www.physics.purdue.edu/astro/MOJAVE/allsources.html>.

References

- Agudo, I., Bach, U., Krichbaum, T.P., Marscher, A.P., Gonidakis, I., Diamond, P.J., Perucho, M., Alef, W., Graham, D.A., Witzel, A., Zensus, J.A., Bremer, M., Acosta-Pulido, J.A., Barrena, R.: Superluminal non-ballistic jet swing in the quasar NRAO 150 revealed by mm-VLBI. *A&A* **476**, 17 (2007)
- Algebra, J.C.: High-frequency very long baseline interferometry rotation measure of eight active galactic nuclei. *MNRAS* **429**, 3551 (2013)
- Aloy, M.A., Ibáñez, J. M., Martí, J. M., Gómez, J.-L., Müller, E.: High-resolution three-dimensional simulations of relativistic jets. *ApJ* **523**, 125 (1999)
- Aloy, M.A., Gómez, J.-L., Ibáñez, J.M., Martí, J.M., Müller, E.: Radio emission from three-dimensional relativistic hydrodynamic jets: Observational evidence of jet stratification. *ApJ* **528**, 95 (2000)
- Aloy, M.A., Martí, J.M., Gómez, J.-L., Agudo, I., Müller, E., Ibáñez, J.M.: Three-dimensional simulations of relativistic precessing jets probing the structure of superluminal sources. *ApJ* **585**, 109 (2003)
- Asada, K., Inoue, M., Uchida, Y., Kamenno, S., Fujiwara, K., Iguchi, S., Mutoh, M.: A helical magnetic field in the jet of 3C 273. *PASJ* **54**, L39 (2002)
- Asada, K., Nakamura, M., Inoue, M., Kamenno, S., Nagai, H.: Multi-frequency polarimetry toward S5 0836+710: A possible spine-sheath structure for the jet. *ApJ* **720**, 41 (2010)
- Attridge, J.M., Roberts, D.H., Wardle, J.F.C.: Radio jet-ambient medium interactions on parsec scales in the blazar 1055+018. *ApJ* **518**, 87 (1999)
- Blandford, R.D.: *Astrophysical Jets*, p. 26. Cambridge University Press, Cambridge (1993)
- Blandford, R.D., Königl, A.: Relativistic jets as compact radio sources. *ApJ* **232**, 34 (1979)
- Bloom, S.D., Fromm, C.M., Ros, E.: The accelerating jet of 3C 279. *AJ* **145**, 12 (2013)

- Blundell, K.M., Bowler, M.G.: Symmetry in the changing jets of SS 433 and its true distance from us. *ApJ* **616**, 159 (2004)
- Britzen, S., Witzel, A., Krichbaum, T.P., Beckert, T., Campbell, R.M., Schalinski, C., Campbell, J.: The radio structure of S5 1803+784. *MNRAS* **362**, 966 (2005)
- Broderick, A.E., McKinney, J.C.: Parsec-scale faraday rotation measures from general relativistic magnetohydrodynamic simulations of active galactic nucleus jets. *ApJ* **725**, 750 (2010)
- Burn, B.J.: On the depolarization of discrete radio sources by Faraday dispersion. *MNRAS* **133**, 67 (1966)
- Caproni, A., Abraham, Z.: Precession in the inner jet of 3C 345. *ApJ* **602**, 625 (2004a)
- Caproni, A., Abraham, Z.: Can long-term periodic variability and jet helicity in 3C 120 be explained by jet precession? *MNRAS* **349**, 1218 (2004b)
- Caproni, A., Abraham, Z., Monteiro, H.: Monteiro, parsec-scale jet precession in BL lacertae (2200+420). *MNRAS* **428**, 280 (2013)
- Cawthorne, T.V., Cobb, W.K.: Linear polarization of radiation from oblique and conical shocks. *ApJ* **350**, 536 (1990)
- Cawthorne, T.V., Hughes, P.A.: The radiative transfer of synchrotron radiation through a compressed random magnetic field. *ApJ* **77**, 60 (2013)
- Cawthorne, T.V., Jorstad, S.G., Marscher, A.P.: Polarization structure in the core of 1803+784: A signature of recollimation shocks? *ApJ* **772**, 14 (2013)
- Cohen, M.H., Lister, M.L., Homan, D.C., Kadler, M., Kellermann, K.I., Kovalev Y. Y, Vermeulen, R. C.: Relativistic beaming and the intrinsic properties of extragalactic radio jets. *ApJ*, **658**, 232 (2007)
- Cohen, M.H., Meier, D.L., Arshakian, T.G., Homan, D.C., Hovatta, T., Kovalev, Y.Y., Lister, M.L., Pushkarev, A.B., Richards, J.L., Savolainen, T.: Studies of the jet in bl lacertae. I. recollimation shock and moving emission features. *ApJ* **787**, 151 (2014)
- Coughlan, C.P.: The development of new methods for high resolution radio astronomy imaging, PhD Thesis, University College Cork, Ireland (2014)
- Contopoulos, I., Christodoulou, D.M., Kazanas, D., Gabuzda, D.C.: The invariant twist of magnetic fields in the relativistic jets of active galactic nuclei. *ApJL* **702**, L148 (2009)
- Croke, S.M., Gabuzda, D.C.: Aligning VLBI images of active galactic nuclei at different frequencies. *MNRAS* **386**, 619 (2008)
- Croke, S.M., O'Sullivan, S.P., Gabuzda, D.C.: The parsec-scale distributions of intensity, linear polarization and Faraday rotation in the core and jet of Mrk501 at 8.4-1.6 GHz. *MNRAS* **402**, 259 (2010)
- Gabuzda, D.C., Gómez, J.-L.: iVSOP polarization observations of the BL Lacertae object OJ 287. *MNRAS* **320**, 49 (2001)
- Gabuzda, D.C., Mullan, C.M., Cawthorne, T.V., Wardle, J.F.C., Roberts, D.H.: Evolution of the millisecond total intensity and polarization structures of BL Lacertae objects. *ApJ* **435**, 140 (1994)
- Gabuzda, D.C., Pushkarev, A.B., Cawthorne, T.V.: Analysis of $\lambda = 6$ cm VLBI polarization observations of a complete sample of northern BL lacertae objects. *MNRAS* **319**, 1109 (2000)
- Gabuzda, D.C., Murray, E., Cronin, P.J.: Helical magnetic fields associated with the relativistic jets of four BL Lac objects. *MNRAS* **351**, L89 (2004)
- Gabuzda, D.C., Rastorgueva, E.A., Smith, P.S., O'Sullivan, S.P.: O'Sullivan, Evidence for cospatial optical and radio polarized emission in active galactic nuclei. *MNRAS* **369**, 1596 (2006)
- Gabuzda, D.C., Cantwell, T.M., Cawthorne, T.V.: Cawthorne, magnetic field structure of the extended 3C 380 jet. *MNRAS* **438**, 1 (2013)
- Gabuzda, D.C., Reichstein, A.R., O'Neill, E.L.: Are spine-sheath polarization structures in the jets of active galactic nuclei associated with helical magnetic fields? *MNRAS* (2014, in press)
- Giroletti, M., Giovannini, G., Feretti, L., Cotton, W.D., Edwards, P.G., Lara, L., Marscher, A.P., Mattox, J.R., Piner, B.G., Venturi, T.: Parsec-scale properties of markarian 501. *ApJ* **600**, 127 (2004)
- Gómez, J.-L., Roca-Sogorb, M., Agudo, I., Marscher, A.P., Jorstad, S.G.: On the source of faraday rotation in the jet of the radio galaxy 3c 120. *ApJ* **733**, 11 (2011)

- Homan, D.C.: Inverse Depolarization: A potential probe of internal Faraday rotation and helical magnetic fields in extragalactic radio jets. *ApJ* **747**, 24 (2012)
- Homan, D.C., Lister, M.L.: MOJAVE: Monitoring of jets in active galactic nuclei with VLBA experiments. II. First-Epoch 15 GHz circular polarization results. *AJ* **131**, 1262 (2006)
- Homan, D.C., Wardle, J.F.C.: Detection and measurement of parsec-scale circular polarization in four AGNs. *AJ* **118**, 1942 (1999)
- Homan, D.C., Wardle, J.F.C.: High levels of circularly polarized emission from the radio jet in NGC 1275 (3C 84). *ApJ* **602**, 13 (2004)
- Homan, D.C., Lister, M.L., Kellermann, K.I., Cohen, M.H., Ros, E., Zensus, J.A., Kadler, M., Vermeulen, R.C.: Jet collimation in action: Realignment on kiloparsec scales in 3C 279. *ApJ* **589**, 9 (2003)
- Homan, D.C., Attridge J.M., Wardle, J.F.C.: Parsec-scale circular polarization observations of 40 blazars. *ApJ* **556**, 113 (2001)
- Hovatta, T., Valtaoja, E., Tornikoski, M., Lhteenmäki, A.: Doppler factors, Lorentz factors and viewing angles for quasars, BL Lacertae objects and radio galaxies. *A&A* **494**, 527 (2009)
- Hovatta, T., Lister, M.L., Aller, M.F., Aller, H.D., Homan, D.C., Kovalev, Y.Y., Pushkarev, A.B., Savolainen, T.: MOJAVE: Monitoring of jets in active galactic nuclei with VLBA experiments. VIII. Faraday rotation in Parsec-scale AGN jets. *AJ* **144**, 105 (2012)
- Hovatta, T., Aller, M.F., Aller, H.D., Clausen–Brown, E., Homan, D.C., Kovalev, Y.Y., Lister, M.L., Pushkarev, A.B., Savolainen, T.: MOJAVE: Monitoring of jets in active galactic nuclei with VLBA experiments. XI. Spectral distributions. *AJ* **147**, 143 (2014)
- Hughes, P.A., Aller, H.D., Aller, M.F.: Polarized radio outbursts in BL Lacertae - part two - the flux and polarization of a piston-driven shock. *ApJ* **298**, 301 (1985)
- Jones, T.W.: Polarization as a probe of magnetic field and plasma properties of compact radio sources - simulation of relativistic jets. *ApJ* **332**, 678 (1988)
- Jones, T.W., O'Dell, S.L.: Transfer of polarized radiation in self-absorbed synchrotron sources. I. Results for a homogeneous source. *ApJ* **214**, 522 (1977)
- Jorstad, S.G., Marscher, A.P., Lister, M.L., Stirling, A.M., Cawthorne, T.V., Gómez, J.-L., Gear, W.K.: Change in speed and direction of the jet near the core in the quasar 3C 279. *AJ* **127**, 3115 (2004)
- Kellermann, K.I., Sramek, R., Schmidt, M., Shaffer, D.B., Green, R.: VLA observations of objects in the Palomar bright quasar survey. *AJ* **98**, 1195 (1989a)
- Kellermann, K.I., Vermeulen, R.C., Zensus, J.A., Cohen, M.H.: Sub-milliarcsecond imaging of quasars and active galactic nuclei. *AJ* **115**, 1295 (1998b)
- Kellermann, K.I., Lister, M.L., Homan, D.C., Vermeulen, R.C., Cohen, M.H., Ros, E., Kadler, M., Zensus, J.A., Kovalev, Y.Y.: Sub-milliarcsecond imaging of quasars and active galactic nuclei. III. Kinematics of parsec-scale radio jets. *ApJ* **609**, 539 (2004)
- Klare, J., Zensus, J.A., Lobanov, A.P., Ros, E., Krichbaum, T.P., Witzel, A.: in *Future Directions in High Resolution Astronomy: The 10th Anniversary of the VLBA*, vol. 340, p. 40. Astronomical Society of the Pacific Conference Proceedings, San Francisco (2005)
- Kovalev, Y.Y., Lobanov, A.P., Pushkarev, A.B., Zensus, J.A.: Zensus, opacity in compact extragalactic radio sources and its effect on astrophysical and astrometric studies. *A&A* **483**, 759 (2008)
- Laing, R.A.: A model for the magnetic-field structure in extended radio sources. *MNRAS* **193**, 439 (1980)
- Legg, M.P.C., Westfold, K.C.: Elliptic polarization of synchrotron radiation. *ApJ* **154**, 499 (1968)
- Lister, M.L., Homan, D.C.: MOJAVE: Monitoring of jets in active galactic nuclei with VLBA Experiments. I. First-Epoch 15 GHz linear polarization images. *AJ* **130**, 1389 (2005)
- Lister, M.L., Aller, H.D., Aller, M.F., Cohen, M.H., Homan, D.C., Kadler, M., Kellermann, K.I., Kovalev, Y.Y., Ros, E., Savolainen, T., Zensus J.A., Vermeulen, R.C.: MOJAVE: Monitoring of jets in active galactic nuclei with VLBA experiments. V. Multi-Epoch VLBA images. *AJ* **137**, 3718 (2009)
- Lobanov, A.P.: Ultracompact jets in active galactic nuclei. *A&A* **330**, 79 (1998)
- Longair, M.S.: High Energy Astrophysics. Cambridge University Press, Cambridge (2010)

- Lovelace, R.V.E., Li, H., Koldoba, A.V., Ustyugova, G.V., Romanova, M.M.: Poynting jets from accretion disks. *ApJ* **572**, 445 (2002)
- Lynden-Bell, D.: Magnetic collimation by accretion discs of quasars and stars. *MNRAS* **279**, L389 (1996)
- Lynden-Bell, D.: On why discs generate magnetic towers and collimate jets. *MNRAS* **341**, 1360 (2003)
- Lyutikov, M.: Role of reconnection in AGN jets. *New Astron. Rev.* **47**, 513 (2003)
- Lyutikov, M., Pariev, V.I., Gabuzda, D.C.: Polarization and structure of relativistic parsec-scale AGN jets. *MNRAS* **360**, 869 (2005)
- Mahmud, M., Gabuzda, D.C., Bezrukovs, V.: Surprising evolution of the parsec-scale Faraday Rotation gradients in the jet of the BL Lac object B1803+784. *MNRAS* **400**, 2 (2009)
- Mahmud, M., Coughlan, C.P., Murphy, E., Gabuzda, D.C., Hallahan, D.R.: Connecting magnetic towers with Faraday rotation gradients in active galactic nuclei jets. *MNRAS* **431**, 695 (2013)
- Marscher, A.P.: Turbulent, extreme multi-zone model for simulating flux and polarization variability in blazars. *ApJ* **780**, 87 (2014)
- Meier, D.L., Koide, S., Uchida, Y.: Magnetohydrodynamic production of relativistic jets. *Science* **291**, 84 (2001)
- Mimica, P., Aloy, M.A.: On the dynamic efficiency of internal shocks in magnetized relativistic outflows. *MNRAS* **401**, 525 (2010)
- Mimica, P., Aloy, M.A.: Radiative signature of magnetic fields in internal shocks. *MNRAS* **421**, 2635 (2012)
- Murphy, E., Cawthorne, T.V., Gabuzda, D.C.: Analysing the transverse structure of the relativistic jets of active galactic nuclei. *MNRAS* **430**, 1504 (2013)
- Murphy, E., Gabuzda, D.C.: The innermost regions of relativistic jets and their magnetic fields. *EPJ Web Conf.* **61**, id.07005 (2013)
- Nakamura, M., Uchida, Y., Hirose, S.: Production of wiggled structure of AGN radio jets in the sweeping magnetic twist mechanism. *New Astron.* **6**, 61 (2001)
- O'Sullivan, S.P., Gabuzda, D.C.: Magnetic field strength and spectral distribution of six parsec-scale active galactic nuclei jets. *MNRAS* **400**, 260 (2009)
- Pacholczyk, A.G.: *Radio Astrophysics*. Freeman, San Francisco (1970)
- Papageorgiou, A., Cawthorne, T.V., Stirling, A., Gabuzda, D., Polatidis, A.G.: Space very long baseline interferometry observations of polarization in the jet of 3C380. *MNRAS* **373**, 449 (2006)
- Pariev, V.I., Istomin, Ya.N., Beresnyak, A.R.: Relativistic parsec-scale jets: II. Synchrotron emission. *A&A* **403**, 805 (2003)
- Pushkarev, A.B., Gabuzda, D.C., Vetukhnovskaya, Yu.N., Yakimov, V.E.: Spine-sheath polarization structures in four active galactic nuclei jets. *MNRAS* **356**, 859 (2005)
- Pushkarev, A.B., Hovatta, T., Kovalev, Y.Y., Lister, M.L., Lobanov, A.P., Savolainen, T., Zensus, J.A.: MOJAVE: Monitoring of jets in active galactic nuclei with VLBA experiments. IX. Nuclear opacity. *A&A* **545**, 113 (2012)
- Qian, S.-J., Witzel, A., Zensus, J.A., Krichbaum, T.P., Britzen, S., Zhang, X.-Zh.: Periodicity of the ejection of superluminal components in 3C345. *Res. Astron. Astrophys.* **9**, 137 (2009)
- Rybicki, G.B., Lightman, A.P.: *Radiative processes in astrophysics*. Wiley, New York (1979)
- Sikora, M., Begelman, M.C., Madejski, G.M., Lasota, J.-P.: Lasota, are quasar jets dominated by poynting flux? *ApJ* **625**, 62 (2005)
- Sokolovsky, K.V., Kovalev, Y.Y., Pushkarev, A.B., Lobanov, A.P.: A VLBA survey of the core shift effect in AGN jets. I. Evidence of dominating synchrotron opacity. *A&A* **532**, 38 (2011)
- Stirling, A.M., Cawthorne, T.V., Stevens, J.A., Jorstad, S.G., Marscher, A.P., Lister, M.L., Gómez, J.-L., Smith, P.S., Agudo, I., Gabuzda, D.C., Robson, E.I., Gear, W.K.: Discovery of a precessing jet nozzle in BL Lacertae. *MNRAS* **341**, 405 (2003)
- Taylor, G.B.: Magnetic fields in quasar cores. *ApJ* **506**, 637 (1998)
- Taylor, G.B.: Magnetic fields in quasar cores. II. *ApJ* **533**, 95 (2000)
- Taylor, G.B., Zavala, R.: Are there rotation measure gradients across active galactic nuclei jets? *ApJ* **722**, 183 (2010)

- Tsinganos, K., Bogovalov, S.: Magnetic collimation of relativistic outflows in jets with a high mass flux. *MNRAS* **337**, 553 (2002)
- Vitrishchak, V.M., Gabuzda, D.C.: New measurements of the circular polarization of the radio emission of active galactic nuclei on parsec scales, *Astron. Rep.* **51**, 695 (2007)
- Vitrishchak, V.M., Gabuzda, D.C., Algaba, J.C., Rastorgueva, E.A., O'Sullivan, S.P., On'Dowd, A.: The 15-43 GHz parsec-scale circular polarization of 41 active galactic nuclei. *MNRAS* **391**, 124 (2008)
- Walker, R.C., Dhawan, V., Romney, J.D., Kellermann, K.I., Vermeulen, R.C.: VLBA absorption imaging of ionized gas associated with the accretion disk in NGC 1275. *ApJ* **530**, 233 (2000)
- Wardle, J.F.C., Homan, D.C.: Laing, R.A., Blundell, K. (eds.) *Particles and Fields in Radio Galaxies*. Astronomical Society of the Pacific Conference Series vol. 250, p. 15 (2001)
- Wardle, J.F.C., Homan, D.C.: Circular polarisation from relativistic jet sources. *Astrophys. Space Sci.* **288**, 143 (2003)
- Zavala, R.T., Taylor, G.B.: A view through faraday's fog: Parsec-scale rotation measures in active galactic nuclei. *ApJ* **589**, 126 (2003)
- Zavala, R.T., Taylor, G.B.: A View through faraday's fog. II. Parsec-scale rotation measures in 40 active galactic nuclei. *ApJ* **612**, 749 (2004)
- Zensus, J.A., Rosn, E., Kellermann, K.I., Cohen, M.H., Vermeulen, R.C., Kadler, M.: Sub-milliarcsecond imaging of quasars and active galactic nuclei. II. Additional sources. *AJ* **124**, 662 (2002)